Technical Report
for Project Titled

"Neutralizing Carbonic Acid in Deep Carbonate Strata below the North Atlantic"

Annual Technical Report for Period July 15, 2005 – July 14, 2006

Principal Investigator: Daniel P. Schrag

October 12 2006

DOE Award Number DE-FG26-04NT42123

Submitted by:

President and Fellows of Harvard College
Department of Earth and Planetary Sciences
Suite 727
Cambridge, MA 02138-2902

ABSTRACT

Our research is aimed at investigating several technical issues associated with carbon dioxide sequestration in calcium carbonate sediments below the sea floor through laboratory experiments and chemical transport modeling. Our goal is to evaluate the basic feasibility of this approach, including an assessment of optimal depths, sediment types, and other issues related to site selection. The results of our modeling efforts were published this past summer in the Proceedings of the National Academy of Sciences. We are expanding on that work through a variety of laboratory and modeling efforts. In the laboratories at Columbia and at Harvard, we are studying the flow of liquid carbon dioxide and carbon dioxide-water mixtures through calcium carbonate sediments to better understand the geomechanical and structural stability of the sediments during and after injection. We are currently preparing the results of these findings for publication. In addition, we are investigating the kinetics of calcium carbonate dissolution in the presence of CO_2 -water fluids, which is a critical feature of the system as it allows for increased permeability during injection. We are also investigating the possibility of carbon dioxide hydrate formation in the pore fluid, which might complicate the injection procedure by reducing sediment permeability but might also provide an upper seal in the sediment-pore fluid system, preventing release of CO_2 into the deep ocean, particularly if depth and temperature at the injection point rule out immediate hydrate formation. This is done by injecting liquid CO2 into various types of porous media, and then monitoring the changes in permeability. Finally, we are performing an economic analysis to estimate costs of drilling and gas injection, site monitoring as well as the availability of potential disposal sites with particular emphasis on those sites that are within the 200-mile economic zone of the United States. We present some preliminary results from these analyses. A paper discussing the site selection based on data from the Ocean Drilling Program and Deep Sea Drilling Program is currently in preparation.

TABLE OF CONTENTS

LIST OF GRAPHICAL MATERIALS

INTRODUCTION

Our research is aimed at investigating several technical issues associated with carbon dioxide sequestration in calcium carbonate sediments below the sea floor through laboratory experiments and chemical transport modeling. Our goal is to evaluate the basic feasibility of this approach, including an assessment of optimal depths, sediment types, and other issues related to site selection. Through laboratory and modeling efforts, we are studying the flow of liquid carbon dioxide and carbon dioxide-water mixtures through calcium carbonate sediments to better understand the geomechanical and structural stability of the sediments during and after injection. In addition, we are investigating the kinetics of calcium carbonate dissolution in the presence of CO_2 -water fluids, which is a critical feature of the system as it allows for increased permeability during injection. We are also investigating the possibility of carbon dioxide hydrate formation in the pore fluid, which might complicate the injection procedure by reducing sediment permeability but might also provide an upper seal in the sediment-pore fluid system, preventing release of CO_2 into the deep ocean, particularly if depth and temperature at the injection point rule out immediate hydrate formation. Finally, we are performing an economic analysis to estimate costs of drilling and gas injection, site monitoring as well as the availability of potential disposal sites with particular emphasis on those sites that are within the 200-mile economic zone of the United States.

This project is a collaboration between Dan Schrag and his group at Harvard University and Klaus Lackner and his group at Columbia University. In addition, there are several other collaborators, including Charles Harvey, Professor of Hydrology at MIT, who is playing a critical role in the project, and Bruce Watson from RPI who is working with the group on some high pressure experiments. This year was the first one in which Harvey and Watson received funding from the project, and this re-allocation has yielded substantial benefit that will be discussed below.

During this second year of funding, we have made considerable progress on all the various aspects of the project. Our major accomplishment was the completion of an article which has been published in the Proceedings of the National Academy of Sciences that reports the results of our calculations and findings thus far. This paper describes the basic physical and chemical issues associated with injection of liquid CO2 beneath the sea floor, and has attracted considerable attention from various media around the world. Schrag gave an invited talk at a recent conference at Yale University in April, 2006, and also presented this approach at the Stanford Annual Conference for their Global Climate and Energy Program, funded by Exxon-Mobil, Schlumberger, GE and Toyota. For the purposes of this technical report, our results and discussion can be divided into three parts: modeling of fluid flow and chemical reactions during injection of CO2; experimental measurements of kinetics of chemical reactions and permeabilities and dynamics of liquid CO2 injection into sediments; and economic analysis of deep sea injection and comparison with other approaches in a geographic context.

EXECUTIVE SUMMARY

Our research is aimed at investigating several technical issues associated with carbon dioxide sequestration in calcium carbonate sediments below the sea floor through laboratory experiments and chemical transport modeling. Our goal is to evaluate the basic feasibility of this approach, including an assessment of optimal depths, sediment types, and other issues related to site selection. Through laboratory and modeling efforts, we are studying the flow of liquid carbon dioxide and carbon dioxide-water mixtures through calcium carbonate sediments to better understand the geomechanical and structural stability of the sediments during and after injection. In addition, we are investigating the kinetics of calcium carbonate dissolution in the presence of CO_2 -water fluids, which is a critical feature of the system as it allows for increased permeability during injection. We are also investigating the possibility of carbon dioxide hydrate formation in the pore fluid, which might complicate the injection procedure by reducing sediment permeability but might also provide an upper seal in the sediment-pore fluid system, preventing release of CO_2 into the deep ocean, particularly if depth and temperature at the injection point rule out immediate hydrate formation. Finally, we are performing an economic analysis to estimate costs of drilling and gas injection, site monitoring as well as the availability of potential disposal sites with particular emphasis on those sites that are within the 200-mile economic zone of the United States.

During this second year of funding, we have made considerable progress on all the various aspects of the project. Our major accomplishment was the publication of an article in the Proceedings of the National Academy of Sciences that reports the results of our calculations and findings thus far. This paper (which we are unable to attach as an appendix to this report because DOE rules prohibit our including published material in this report) describes the basic physical and chemical issues associated with injection of liquid CO2 beneath the sea floor, and attracted considerable attention in the media. Dan Schrag, the P.I., was invited to present these results as a keynote talk in Stanford's annual conference for their Global Climate and Energy Project (funded by Exxon-Mobil, Schlumberger, Toyota, and GE).

Our work on modeling of the fluid flow associated with CO2 injection into sediments has proceeded as planned. This work is the major component of the Ph.D. thesis of Kurt House, graduate student at Harvard with Dan Schrag. Our basic modeling of CO2 injection into sediments revealed that there are several different components of the flow including 1) basic buoyancy issues of the CO2 plume relative to the pore fluid within a local geothermal gradient, 2) hydrate formation and its effect on limiting permeability and upward migration of a CO2 plume, 3) convection within the CO2 plume due to the high thermal expansion coefficient of liquid CO2, and 4) downward flow of pore fluid saturated in CO2 once it has encountered the CO2 plume. Simple calculations show that all these processes are important on various timescales, but that the downward advection of water saturated with CO2 will ultimately determine the fate of CO2 sequestered in deep sea sediments, with the final state being a diffuse plume of CO2-saturated water sitting between 300 and 500 meters below the sea floor. Kurt is currently extending his results from the simpler models to more sophisticated reservoir models provided by Schlumberger, who will collaborate with us on the project. Charles Harvey, a hydrologist from MIT, is assisting with this modeling effort. A publication from this effort should be submitted by the end of this academic year.

The experimental component of the proposal involved measurements of reaction kinetics associated with carbonate dissolution in CO2 rich fluids. Because our calculations have

shown that carbonate dissolution is likely to be important only for the permeability – and then only to a minor extent – our experimental focus has been on identifying complications associated with permeability in these systems, and also measuring rates of hydrate formation and dissolution. Our major goal for Year 2 was to design a high pressure experimental apparatus that would allow us to measure reaction kinetics and permeability changes at 300 bars pressure or greater. This has been accomplished, in collaboration with Schlumberger, and experiments are currently underway. These experiments are being led by Klaus Lackner and Juerg Matter from Columbia, with colleagues at Schlumberger. Kurt House is assisting with some of the experiments as well.

An additional experimental component of our project is the involvement of Bruce Watson from RPI, a member of the National Academy of Sciences and a superb high pressure experimentalist. Watson has spent this year designing and constructing a static high pressure experimental system to look at chemical kinetics and fluid mechanics at pressure but in a different manner than the flow through system we described in our original proposal, and what the Columbia group is doing with Schlumberger. These experiments, which should produce the first results this winter, will complement the flow through results and will be very important in constraining rates and key processes such as interaction between carbonates and hydrates.

The final component of our project can be broadly characterized as an economic assessment, although this includes a variety of other activities including site surveys. We have examined the 25 cores from the Deep Sea Drilling Project and Ocean Drilling Program that are most relevant to injecting CO2 into deep sea sediments. We are using the chemical and physical properties from these sites to aid the choices in our modeling and experimental efforts. Graduate student Jeff Bielicki is finishing an economic analysis of the costs of sequestration in deep sea sediments, including estimates of where in the US this approach might be most efficient. We expect to have a report on costs of this approach by the end of the summer. Bielicki and Schrag have also completed a manuscript that grew out of this work on optimizing locations of new coal plants with carbon capture capability based on the trade-offs between distance to site of sequestration and distance to the consumer of electricity. Bielicki presented these results this past summer in Europe at the Carbon Sequestration Conference.

EXPERIMENTAL

There are two main experimental efforts associated with this project. One of them is aimed at measuring permeability of deep sea sediments to liquid CO2 injection. Apparatus for making these measurements has been constructed at Columbia, at Harvard, and we are also working on a similar apparatus at Schlumberger's labs in Ridgefield, Connecticut (soon to be moving to Cambridge, MA). Methods used at all locations are very similar. All involve a high pressure CO2 source that is injected at constant flow rate into a porous medium – either actual core samples of deep sea sediment or synthetic material designed for more idealized tests. The source of CO2 is a high-precision liquid CO2 pump that can maintain constant flow rate of liquid CO2 and maintain a set temperature over a very wide range of pressures. The simple experiments being done at Harvard use idealized porous media to understand the effects of hydrate formation on permeability. The methods used at Columbia are more complex, as they are focused on making measurements from core samples in sediments that are similar to what we propose as an injection site. The final experimental effort associated with this project is the high-pressure system currently being designed by Bruce Watson at RPI. As this is the first year of his funding in this project, the experimental methods are still being worked out. A more complete methods description will be provided in the third year report.

RESULTS AND DISCUSSION

Modeling of Injection of CO2 in Deep Sea Sediments:

Our work on modeling of the fluid flow associated with CO2 injection into sediments has proceeded as planned. This work is the major component of the Ph.D. thesis of Kurt House, graduate student at Harvard with Dan Schrag. Kurt's initial approach was to use very simple fluid flow models to explore some of the interesting fluid mechanics associated with liquid CO2 injection. These calculations revealed that there are several different components of the flow including 1) basic buoyancy issues of the CO2 plume relative to the pore fluid within a local geothermal gradient, 2) hydrate formation and its effect on limiting permeability and upward migration of a CO2 plume, 3) convection within the CO2 plume due to the high thermal expansion coefficient of liquid CO2, and 4) downward flow of pore fluid saturated in CO2 once it has encountered the CO2 plume. Simple calculations show that all these processes are important on various timescales, but that the downward advection of water saturated with CO2 will ultimately determine the fate of CO2 sequestered in deep sea sediments, with the final state being a diffuse plume of CO2-saturated water sitting between 300 and 500 meters below the sea floor. The next step in Kurt's thesis project is to apply more sophisticated modeling tools to this problem. This is currently underway, in collaboration with Schlumberger using their reservoir simulating software (ECLIPSE). We were encouraged to pursue this collaboration with Schlumberger during the review of this project last October, and we are happy to report that we have established a strong relationship and Schlumberger has shown great interest in this work. Schlumberger has recently moved one of their main research laboratories from Ridgefield, Connecticut to Cambridge, Massachusetts, which greatly facilitates our collaboration. Charles Harvey, a hydrologist from MIT, is assisting with this modeling effort. We expect we will have publishable results on the modeling effort this year, but we have already a variety of findings from the simpler models that will be discussed below.

Due to the high compressibility of CO_2(l) relative to water, CO_2(l) becomes denser than water at high pressures and low temperatures. These temperature-pressure regimes do not exist in terrestrial settings; they are, however, common in the deep ocean. When CO_2(l) is injected into the ocean at a depth of 3000 m, it sinks, forming a lake of CO_2(l) on the seafloor. Ocean currents, however, can mix the injected CO_2(l) causing a large fraction to eventually be released into the atmosphere (1). To ensure that deep ocean currents will not mix the CO_2 into shallower regions, CO_2 can be injected below the seafloor. Furthermore, if the seafloor depth of injection is greater than ~3000 m, then the injected CO_2 will be denser than the ambient pore-fluid.

We refer to the sub-seafloor region with low enough temperatures and high enough pressures to compress CO_2 to greater density than seawater as the Negative Buoyancy Zone (NBZ). When CO_2 is injected beneath the NBZ, the lower density pore-fluid acts as a buoyancy-cap on the system and ensures gravitational stability. The gravitational stability of the system in deep-sea sediments is in contrast with terrestrial geologic storage where the high pressures and *high* temperatures cause the injected supercritical CO_2 to be gravitationally unstable. The buoyancy-cap, provided by the pore water, serves the same purpose in deep-sea sediments as a cap rock serves in terrestrial geologic formations. The buoyancy-cap, however, is superior to a cap rock because conduits in a cap rock enable buoyant CO_2 to escape. In contrast, the gravitational stability provided by the buoyancy-cap guarantees that fractures in the sediment column cannot serve as conduits for the CO_2, and even large geomechanical perturbations—such as earthquakes—cannot cause the CO_2(l) to be released.

The high pressures and low temperatures necessary to compress CO_2(l) to greater density than the pore-fluid are similar to the conditions necessary for CO_2-hydrates to form. We refer to the sub-seafloor region with low enough temperatures and high enough pressures for hydrate formation as the *hydrate formation zone* (HFZ). The HFZ extends from the seafloor downward into the sediment until the temperature rises above the boundary of the hydrate stability field. A comparison that we have performed of the stability conditions for CO_2-hydrates with the CO_2(l) buoyancy-depth relationship reveals that the HFZ overlaps to a great extent with the NBZ. Although the HFZ exists in submarine sediment at seafloor depths of ~400 m, CO_2(l) does not become denser than seawater until a seafloor depth of ~2900 m. Below ~2900 m of ocean, however, the thickness of the NBZ grows more rapidly then the thickness of the HFZ, and at seafloor depths below 4000 m, the NBZ is thicker than the HFZ. The HFZ acts as a second cap on the system as CO_2 below the HFZ will be unable to migrate through the HFZ without forming hydrates, which we believe will severely impede the upward flow of CO_2.

Key Questions Resulting from Initial Findings

A) How will hydrate formation affect the relative permeability of liquid CO_2?

a. How does the timescale of hydrate formation compare with the time scale buoyant flow?

b. How does the increase in salt concentration after the formation of hydrates at the interface of liquid CO_2 and seawater affect the formation of additional hydrates?

c. How effectively will CO_2-hydrates plug pores and limit further migration of CO_2(l)?

e. How the hydrates themselves flow in the pore spaces?

B) How will the post-injection plume evolution depend on the initial temperature of the injected CO_2?

a. We know the plume is unstable at high-enough permeability. Will the instability

create convective mixing of the CO_2(l) plume?

b. What are the time scales for complete hydrate formation, hydrate dissolution, and CO_2 dissolution?

Pore Scale Modeling:

A key question from our initial findings is how the dynamic formation of CO_2-hydrates in porous media will affect the relative permeabilities of CO_2(l) and seawater. In order to answer that question with confidence, we have engaged in parallel tracks of experimentation and numerical modeling of multiphase pore-scale flow in the hydrate stability regimes. Large scale reservoir simulators (i.e., Eclipse or ToughReact) have *not* been built with the capability to model multiphase flow in the presence of hydrate formation. Too little is known about the effects of hydrate formation on relative permeabilities to accurately model large scale plume evolution with CO_2-hydrate formation. We believe that a dynamic pore-scale model coupled with an experiment of CO_2(l) displacing H_2O(l) in a capillary tube will produce the necessary background to build a more complete theory of dynamic hydrate formation in porous media.

At the pore-scale, three forces affect the dynamics of multiphase flow: buoyancy, friction, and capillarity. There are a few key assumptions associated with our dynamic model. In particular, the model is one-dimensional in space and assumes the shape of the meniscus—indicated in part by the wetting angle—is constant. That assumption implies the expectation of a Poiseuille flow distribution within the capillary. This assumption is likely valid as the Reynolds number is $\sim 10^{-2} - \sim 10^{-4}$.

The dynamic model can be solved numerically for any pore geometry by simply applying the necessary geometric relationship $r_1 = r_1(z)$. When these equations are applied to a stochastic pore structure of many pores and many connecting tubes, then the fundamental pore dynamics will in aggregate produce large scale flow patterns. From such a pore-scale model, relative permeabilities curves for reservoir scale simulations can be produced.

We are working on several approaches to integrating hydrate forming into our pore-scale. The simplest approach is to assume that hydrates form on the pore walls, and thus reduce the pore radius as they form. Such a simple model would require r_1 to be a function of the hydrate concentration: $r_1 = r_1(z,[nH_2O \cdot CO_2])$. To calculate the concentration of CO_2-hyrate, we need a thermodynamic model of hydrate formation. There are several thermodynamic models of hydrate formation in the literature that we are using to predict when and where hydrates will form.

Thermal Evolution of the CO_2 Plume and Reservoir-Scale Modeling

In addition to the pore-scale modeling and experimentation, we are engaged in reservoir-scale modeling of the post injection plume and thermal evolution. Until hydrate formation is better understood, the reservoir scale modeling is focusing on the behavior of liquid CO_2 and seawater below both the negative buoyancy zone and the hydrate formation zone. For these purposes, we have partnered with the oil services firm Schlumberger. Schlumberger has invested substantial resources into optimizing its reservoir-scale model of multi-phase porous media flow, and they have granted Harvard University an Eclipse license for these purposes.

Once the initial injection of CO_2(l) is complete, then the system will evolve by several

processes including: buoyancy-driven advection of the CO_2(l), convection within the pure CO_2(l) plume, dissolution of the CO_2(l) into the pore fluid, and dissolution of carbonate host rock,. To model these processes, the equations for multiphase flow in porous media and the chemical relationships associated with the system must be solved simultaneously for an inhomogeneous intrinsic permeability field. As previously mentioned, large investments have gone into writing reservoir models to simulate multiphase flow and chemistry at various reservoir conditions. Eclipse has been optimized for high temperature and high pressure conditions. Therefore, we are working with Schlumberger to extend the Eclipse code to handle the relevant temperature-pressure space.

Schlumberger's Eclipse model solves the standard multiphase flow equations with the empirical relative permeability functions and capillary functions applied to complete the set of equations. For the system of interest, the standard multiphase flow equations must be coupled with the thermal energy balance, the dissolved species balance, and the equations of state for CO_2 and seawater at *low* temperature and *high* pressure. To date, nobody has reliably measured the relative permeability of liquid CO_2 and seawater. Until such measurements are made in reliable ways, then we are relying on relative permeability curves such as the van Gunucten curves for oil and water (3).

As revealed in our PNAS paper, the temperature of the injected CO_2(l)—without an insulated pipe—will be equivalent to the seafloor bottom temperature. That is a potential problem because we will likely need to avoid hydrate formation near the injection point. Avoiding hydrate formation near the well-head will require controlling the temperature at the point of injection. A linear stability analysis indicates that at a high enough intrinsic permeability ($\sim 10^{-13}$ m^2) the saturated CO_2 plume will be unstable. Therefore, the post-injection plume evolution may involve convective mixing of the pure CO_2 plume, which may accelerate the dissolution of the CO_2 liquid phase. Determining the timescales of dissolution through accurate modeling of the CO_2 plume and thermal evolution is an important goal of the Schlumberger-Harvard collaboration.

Experiments of Sediment Permeability and Behavior of Liquid CO2 in Deep Sea Sediments:

To both validate the pore scale model of multiphase flow and to observe the effects of CO_2-hydrate formation on the relative permeabilities, we are building an experiment to observe the flow of CO_2(l) and H_2O in capillary tubes. The first goal of the capillary flow experiment is to validate the dynamic model previous discussed. We are currently validating the model with immiscible fluids that are liquid at surface conditions. Using immiscible fluids that are liquids are surface conditions is a natural step as they are easier to manipulate than fluids—such as CO_2—that must be pressurized and cooled. We are currently injecting oil—the non-wetting phase—into water and measuring the flow characteristics. Upon the completion of the oil-H_2O experiments, CO_2(l) will replace oil as the non-wetting phase being injected into an H_2O saturated capillary tube.

The final step in the pore scale experiment is to place a portion of the capillary tube in a cold bath. The liquid/hydrate/vapor triple point of CO_2 occurs at ~4.5 MPa (~650 psi) and ~9 C. By keeping the pressure above ~4.5 MPa and a portion of the capillary tube below 9 C, we can guarantee hydrate stability at particular point in the capillary tube. We envision running

the experiment with the temperature throughout th e entire capillary tube above the hydrate stability temperature. In the absence of hydrate formation, the position of the meniscus as a function of time should follow the solution to the above dynamic model.

The next step is to decrease the temperature over a portion of the capillary tube. After that decrease in temperature, hydrates will form in the capillary tube. It is not clear how the flow in the capillary tube will change once hydrates start to form. We will, however, have detailed pressure and flow data to indicate how the flow was disrupted by the formation of CO_2-hydrates. It is our goal for the next year to combine that pressure and flow data with the above dynamic model and with existing models of the kinetics and thermodynamics of CO_2-hydrate formation to develop a robust relative permeability model for the CO_2(l)-Hydrate-H_2O system. Ultimately, we intend to upscale this model and integrate it into reservoir-scale simulators.

In addition to the pore-scale experiments, we are also continuing the experimental component of the proposal involved measurements of reaction kinetics associated with carbonate dissolution in CO2 rich fluids. Considerable progress was made on this front during Year 1, and some results from the Columbia group are currently being prepared for publication. However, because our calculations have shown that carbonate dissolution is likely to be important only for the permeability – and then only to a minor extent – our experimental focus has been on identifying complications associated with permeability in these systems, and also measuring rates of hydrate formation and dissolution. Our major goal for Year 2 was to design a high pressure experimental apparatus that would allow us to measure reaction kinetics and permeability changes at 300 bars pressure or greater. This has been accomplished, in collaboration with Schlumberger, and experiments are currently underway. These experiments are being led by Klaus Lackner and Juerg Matter from Columbia, with colleagues at Schlumberger. Kurt House is assisting with some of the experiments as well. A new focus has been the role that CO2 hydrates may play in affecting the permeability. We expect to have results from these high pressure experiments this summer, with at least one publication prepared by next fall. A more detailed description of these experiments is included below:

Porosity, Permeability Analysis:
Formation porosity and permeability are key reservoir parameters needed to define injectability and storage capacity of deep sea sediments for CO_2 sequestration. However, porosity and permeability data is missing at all in the DSDP (Deep Sea Drilling Project) and ODP (Ocean Drilling Project) site and logging databases. Based on the U.S. Atlantic coastline borehole and drilling site database, which was developed during Year I of the project, we collected 45 small (1-inch diameter) cores from various DSDP and ODP cores for porosity and permeability measurements. The core sampling was performed at the Lamont-Doherty Earth Observatory core repository as well as at the ODP core repositories in Texas and Germany (Bremen). Porosity and permeability measurements were performed on ten samples from three different sites in the western Atlantic. The test sites included one site on the New Jersey shelf (Leg 150), one close to the Great Bahama Bank (Leg 166) and one on the Blake Ridge (Leg 11). These sites were chosen because of their end member status with respect to the sedimentology. The samples from the New Jersey shelf are representative of clayey to sandy sediments, whereas the samples from the Blake Ridge are deep sea carbonate oozes and the ones from the Great Bahama Bank are shallow carbonate oozes.

Ten samples from these three sites were tested for brine permeability at specified effective stress. The samples, as a suite, were highly variable, both in terms of their permeabilities and porosities and their textures and physical properties. Some were soft (with the consistency of modeling clay) and visibly deformed during testing, while others are quite competent. In general, their permeabilities were low to intermediate (5 nD to 30 μD). With a wide range of porosities (18 to 47 percent). Due to the low effective stresses, fragile nature of the samples, and the length of time needed to equilibration at stress, no stress dependence of the permeability was measured. Samples were tested saturated with NaCl brines (35,000 ppm) at room temperature. Permeabilities were measured using an AutoLab 1000 test system developed by New England Research, Inc., and capable of automated hydraulic control of confining and pore pressures (Figure 1).

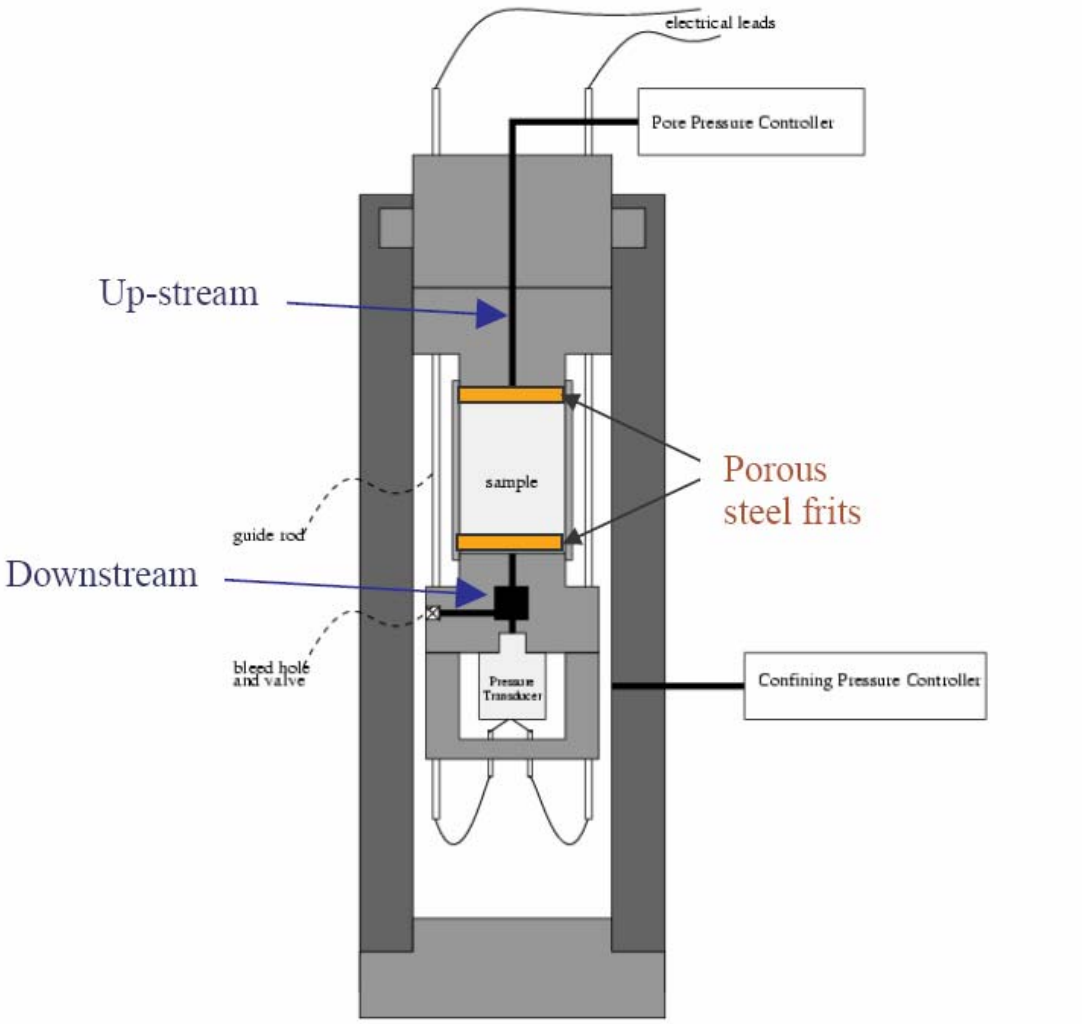

Figure 1: Schematic drawing of the New England Research, Inc. test apparatus (core holder assembly).

The samples were placed in a low dead volume permeability core holder with a 1.3 cc downstream volume monitored by a miniature pressure transducer. Porous steel frits were used to distribute flow to the sample ends without the need for fluid distribution grooves. The samples were loaded to the desired effective stresses by simultaneously ramping the confining and pore pressures to the target conditions. A complex transient method, using the equipment and technique described in Boitnott (1997) was used to measure permeability. The frequency and shape to the transient was tuned to optimize signal to noise for each sample. Data processing was modified to incorporate the effective of storativity on permeability estimation. Once the test was completed, the samples were unloaded slowly to avoid overpressuring the samples. Post-test dimensions and weights were recorded and samples were dried. Dry weights were then recorded and the difference between the computed dry and saturated post-test densities were used to estimate the grain density and porosity. Results of the permeability and porosity measurements are illustrated in Figure 2. The measured permeability and porosity data strongly reflects the heterogeneity of the sediments.

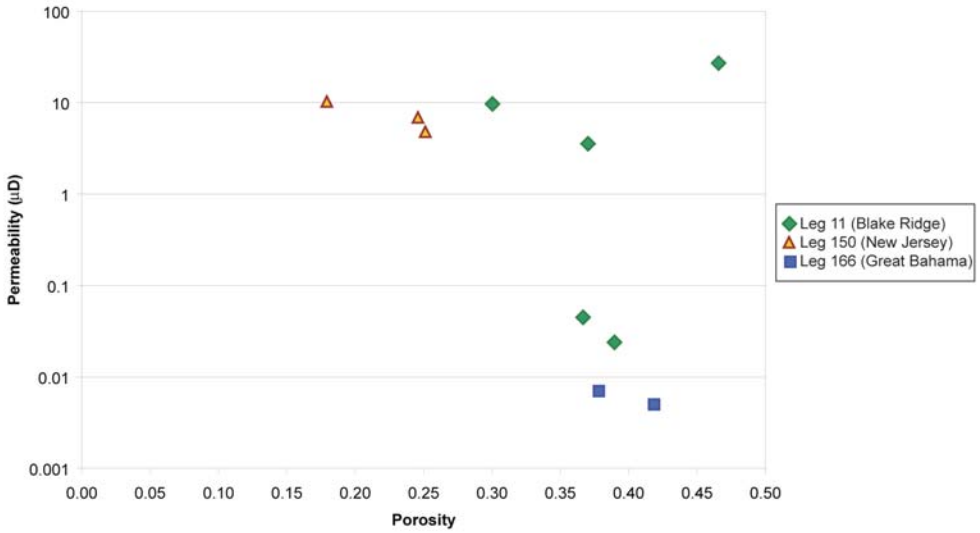

Figure 2: Permeability, porosity data from Leg 11, Leg 150 and Leg 166.

An additional experimental component of our project is the involvement of Bruce Watson from RPI, a member of the National Academy of Sciences and a superb high pressure experimentalist. Watson has spent this year designing and constructing a static high pressure experimental system to look at chemical kinetics and fluid mechanics at pressure but in a different manner than the flow through system we described in our original proposal, and what the Columbia group is doing with Schlumberger. These experiments, which should produce the first results early next year, will complement the flow through results and will be

very important in constraining rates and key processes such as interaction between carbonates and hydrates.

Economic and Site Analysis:

The final component of our project can be broadly characterized as an economic assessment, although this includes a variety of other activities including site surveys. We have examined more than 25 cores from the Deep Sea Drilling Project and Ocean Drilling Program that are most relevant to injecting CO2 into deep sea sediments. We are using the chemical and physical properties from these sites to aid the choices in our modeling and experimental efforts. The sites with most relevant data are shown on the map below. With data from these sites, we will be able, in Year 3, to begin to do some specific site assessments that will represent important steps towards actual field experiments, the logical next step in our project. In addition, graduate student Jeff Bielicki is finishing an economic analysis of the costs of sequestration in deep sea sediments, including estimates of where in the US this approach might be most efficient. A draft of these calculations are attached to this report as Appendix 1. We expect to have a report on costs of this approach by the end of the grant. Bielicki and Schrag have also completed a manuscript that grew out of this work on optimizing locations of new coal plants with carbon capture capability based on the trade-offs between distance to site of sequestration and distance to the consumer of electricity. Bielicki presented these results this summer in Europe at the Carbon Sequestration Conference.

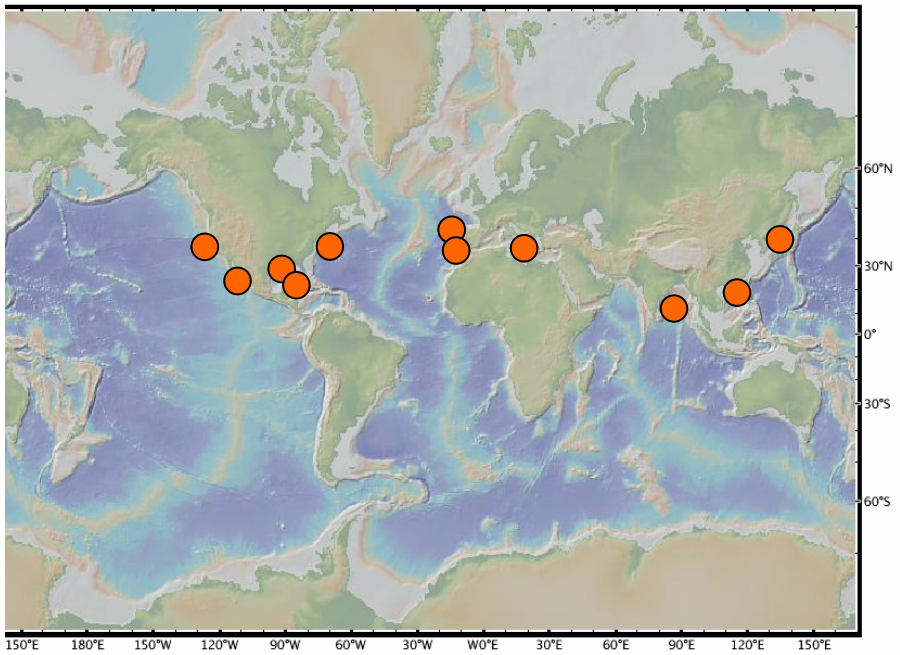

Figure 3: DSDP and ODP Sites from which data on formation factor, porosity, and mineralogy have been obtained for our site assessment.

CONCLUSION

This second year of funding has been a very productive one. We have already accomplished most of our original goals from our original proposal in that we now have a sophisticated understanding of the behavior of liquid CO2 in deep sea sediments, and have also done a rather extensive economic and site analysis. The work has focused our efforts on the behavior of sediments during deformation during injection as permeability has been shown to be a critical issue that may limit the applicability of this method to various sites. The work during Year 3 will help us resolve some outstanding issues, and will provide critical information that can help us formulate a plan for field testing, which we hope to accomplish in a second three year proposal. In general, our results support the idea that injection of CO2 into deep sea sediments is the only truly permanent method of carbon sequestration that has essentially unlimited capacity and is also economically competitive with other methods.

REFERENCES AND BIBLIOGRAPHY

Archer, D., H. Kheshgi, and E. Maier-Reimer, *Multiple timescales for neutralization of fossil fuel CO_2.* Geophysical Research Letters, 1997. **24**(4): p. 405-408.

Bachu, S., W.D. Gunter, and E.H. Perkins, *Aquifer Disposal of CO_2: Hydrodynamic and Mineral Trapping.* Energy Convers. Mgmt., 1994. **35**(4): p. 269–279.

Bergman, P.D. and E.M. Winter, *Disposal of CO2 in aquifers in the US.* Energy Convers. Mgmt, 1995. **36**: p. 523-526.

Broecker, W.S. and T. Takahashi, *Neutralization of Fossil Fuel CO_2 by Marine Calcium Carbonate*, in *The Fate of Fossil Fuel CO_2 in the Oceans*, N.R. Andersen and A. Malahoff, Editors. 1978, Plenum Publishing Corporation: New York.

Caldeira, K. and G.H. Rau, *Accelerating carbonate dissolution to sequester carbon dioxide in the ocean: Geochemical implications.* Geophysical Research Letters, 2000. **27**(2): p. 225-228.

Caldeira K, Wickett ME, Duffy PB, *Depth, radiocarbon, and the effectiveness of direct CO2 injection as an ocean carbon sequestration strategy***,** Geophysical Research Letters, 2002, **29** (16): art. no. 1766, 2002.

Hollister, C. D., Ewing, J. I., et al. 1972. Initial Reports of the Deep Sea Drilling Project, Vol. XI. Washington (U.S. Government Printing Office), 219-270

Holloway, S., *Storage of fossil fuel-derived carbon dioxide beneath the surface of the earth.* Annual Review of Energy and the Environment, 2001. **26**: p. 145-166.

Kaszuba, J.P., D.R. Janecky, and M.G. Snow, *Carbon dioxide reaction processes in a model brine aquifer at 200 ℃ and 200 bars: implications for geologic sequestration of carbon.* Applied Geochemistry, 2003. **18**(7): p. 1065-1080.

Koide, H. Y., Shindo, Y., Takzaki, Y., Iijima, M., Ito, K., Kimura, N., and K. Omata (1997). Deep sub-seabed disposal of CO2 - the most protective storage. Energy Conservation Mgmt. 38: S253-S258

Lackner, K.S., *Carbonate Chemistry for Sequestering Fossil Carbon.* Annu. Rev. Energy Environ., 2002. **27**(1): p. 193-232.

McDuff R.E. and Gieskes J.M. (1976) Calcium and magnesium profiles in DSDP interstitial waters: diffusion or reaction? *Earth Planet. Sci. Lett.* **33**, 1-10.

Melim, L. A., Anselmetti, F. S., and G. P. Eberli. (2001). The importance of pore type on permeability of neogene carbonates, Great Bahama Bank. In: Subsurface geology of a prograding carbonate platform margin, Great Bahama Bank: Results of the Bahamas Drilling Project. SEPM Special Publication No. 70.

Nunn JA, Meulbroek P, *Kilometer-scale upward migration of hydrocarbons in geopressured sediments by buoyancy-driven propagation of methane filled fractures,* **AAPG BULLETIN**, 2002, 86 (5): 907-918

Schrag D.P., DePaolo D.J. and Richter F.M. (1992) Oxygen isotope exchange in a two-layer model of oceanic crust. *Earth Planet. Sci. Lett.* **111**, 305-317.

Van Hinte, J. E., Wise, S. W., et al. 1987. Init. Repts. DSDP, 93: Washington (U.S. Govt. Printing Office), Vol. XCIII; Part 1.

Hollister, C. D., Ewing, J. I., et al. 1972. Initial Reports of the Deep Sea Drilling Project, Vol. XI. Washington (U.S. Government Printing Office), 219-270

McDuff R.E. and Gieskes J.M. (1976) Calcium and magnesium profiles in DSDP interstitial waters: diffusion or reaction? *Earth Planet. Sci. Lett.* **33**, 1-10.

Melim, L. A., Anselmetti, F. S., and G. P. Eberli. (2001). The importance of pore type on permeability of neogene carbonates, Great Bahama Bank. In: Subsurface geology of a prograding carbonate platform margin, Great Bahama Bank: Results of the Bahamas Drilling Project. SEPM Special Publication No. 70.

Schrag D.P., DePaolo D.J. and Richter F.M. (1992) Oxygen isotope exchange in a two-layer model of oceanic crust. *Earth Planet. Sci. Lett.* **111**, 305-317.

Van Hinte, J. E., Wise, S. W., et al. 1987. Init. Repts. DSDP, 93: Washington (U.S. Govt. Printing Office), Vol. XCIII; Part 1

LIST OF ACRONYMS AND ABBREVIATIONS

ODP Ocean Drilling Program
DSDP Deep Sea Drilling Project

APPENDIX 1

Appendix for Organization and Intervention in Human-Environment Systems: Deliberate Carbon Capture and Storage in Human-Environment Systems

Jeffrey M. Bielicki

May 23, 2006

A Equations

A.1 Quantity of $CO_{2(l)}$ that can be Stored Deep Sea Sediment

Each location on the surface of the ocean will have an ocean depth (d_{ocean}) and sediment thickness (b_{sed}), porosity (n_{sed}), and intrinsic permeability (κ_{sed}) associated with it. Let a unit area of the ocean floor associated with location l be $A_l(d_{ocean}, b_{sed}, n_{sed}, \kappa_{sed})$. The amount of $CO_{2(l)}$ that can be stored in A_l depends on the thickness of the sediment that can be utilized, the porosity (n_{sed}) of the sediment, and the density of $CO_{2(l)}$ at that depth and thickness.

Assuming a geothermal gradient of 0.03°K/m, a linear approximation of the density of a droplet $CO_{2(l)}$ ($\rho_{CO_{2(l)}}$), at ocean depths greater than -2500 m, is:[1]

$$\rho_{CO_{2(l)}} \cong 1011 - \frac{1}{30} \cdot \left(d_{ocean} + 2000\right) - \frac{11}{175} \cdot \left(b_{sed}\right) \tag{1}$$

where d_{ocean} is a negative value for the depth of the ocean in meters and b_{sed} is the height of the sediment above the droplet of $CO_{2(l)}$ in meters.

The thickness of the sediment that can be utilized for permanent long term $CO_{2(l)}$ storage depends on d_{ocean}. As d_{ocean} increases, the density of $CO_{2(l)}$ ($\rho_{CO_{2(l)}}$) increases more rapidly than that of seawater, but the geothermal gradient within the sediment causes $CO_{2(l)}$ to expand more rapidly than the surrounding pore fluid. A Negative Buoyancy Zone (NBZ) results, extending some depth into the sediment, in which the vertical migration of $CO_{2(l)}$ will be impeded by the changes in density of $CO_{2(l)}$ relative to that of the surrounding seawater. $CO_{2(l)}$ is 'trapped' in the NBZ.

At appropriate ocean depths, $CO_{2(l)}$ will also be 'trapped' by the formation of $CO_{2(l)}$ hydrates in the ocean sediment. These hydrates are crystalline type structures formed by the interaction between CO_2, water, high pressure, and cold temperature. The zone in which a $CO_{2(l)}$ hydrate forms is referred to as the Hydrate Formation Zone, HFZ.

The thickness of the sediment that can be utilized to store $CO_{2(l)}$ constrains the quantity of $CO_{2(l)}$ that can be stored in deep sea sediment: b_{sed} to be bounded by the upper envelope of the NBZ and the HFZ. Linear approximations of these zones are shown in Figure 1, where the shaded portion indicates where $CO_{2(l)}$ will accumulate over the long term and represents the relevant sediment thickness / ocean depth combinations for storage capacity calculations.

For (d_{ocean}) between -3,000 m and -5,500 m, linear approximations of the thicknesses of the NBZ and HFZ are:

$$NBZ_{thickness} = 54 - \frac{73}{270}(depth + 3000) \tag{2}$$

[1] The articulation of density, HFZ, and NBZ is adapted from House et al. (2006).

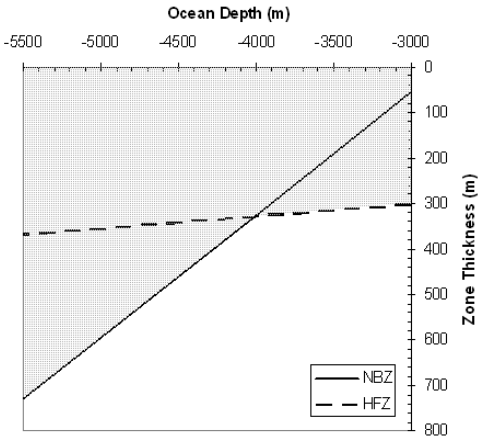

Figure 1: Approximations of Hydrate Formation Zone (HFZ) and Negative Bouyancy Zone (NBZ). (The values of the zone thickness are reversed to convey the depth into the sediment.) Linearized from House et al. (2006).

$$HFZ_{thickness} = 300 - \frac{7}{250}(depth + 3000) \tag{3}$$

For depths between -3,000 m and -4,000 m, the HFZ thickness bounds b_{sed} and below -4,000 m, the NBZ bounds b_{sed}.

Let $\sigma_{CO_{2(l)}}$ be (1) integrated over the total applicable sediment thickness, defined by either (2) or (3), to yield the column integrated amount of $CO_{2(l)}$ that can be stored under a unit area of the ocean floor that is at least 3,000 meters deep:

$$\sigma_{CO_{2(l)}} = \int_0^{b_{sed}} \rho_{CO_{2(l)}}(b_{sed}, d_{ocean}) db_{sed} \tag{4}$$

Integrating (4) over b_{sed} and d_{ocean} for a given areal footprint and multiplying by the available pore space, n, in that area, in the ocean yields the total quantity of $CO_{2(l)}$ that can be stored at that site K_{site}.

$$K_{CO_{2(l)},site} = \int_{A_l} \left(\sigma_{CO_{2(l)}} n\right) dA_l \tag{5}$$

A.2 Pressure Required to Store $CO_{2(l)}$ in Deep Sea Sediment

The pressure necessary to store CO_2 in deep sea sediment equals the hydrostatic pressure at the depth of injection plus the backpressure that results from injecting a fluid into a porous medium. The hydrostatic pressure is simply $P_{hydro} = \rho_{H_2O} g z$, where g is the acceleration due to gravity [9.8 m/s^2] and z is the distance below the ocean surface (ocean depth plus depth into the sediment). The backpressure is determined by the Theis solution for a confined well.[2] The head (dh) required for storage of a compressible fluid in a compressible porous medium is:

$$dh = \frac{Q}{4\pi T} \cdot ln\left(\frac{2.25Tt}{r^2 S}\right) \tag{6}$$

where Q is the volumetric flow rate [m^3/s], t is time [s], T is the transmissivity defined in (7) and S is the storage coefficient defined in (8):

[2]Kurt House provided this formulation of the Theis solution.

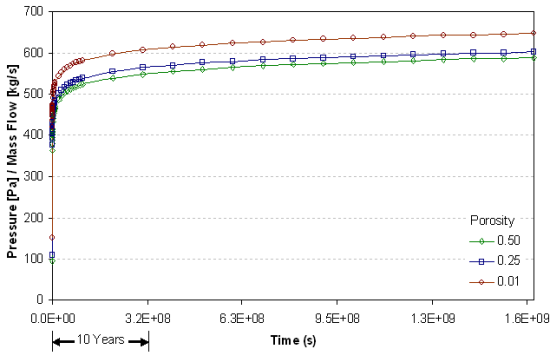

Figure 2: CO_2 Storage in Deep Sea Sediment for Typical Parameters ($\mu = 1 \times 10^{-4}$ Ns/m^2, $\kappa = 10^{-12}$ m^2, $\alpha = 10^{-10}$ m^2/N, $\beta = 3 \times 10^{-9}$ m$^2/N$, $\rho = 1050$ kg/m^3, $b = 325$ m, $r = 0.5$ m)

$$T = \frac{\kappa \rho g b}{\mu} \tag{7}$$

$$S = \rho g b \big(\alpha + n\beta\big) \tag{8}$$

where κ is the intrinsic permeability of the porous medium [m^2], ρ is the density of the injected fluid [kg/m^3], b is the thickness of the porous medium, μ is the viscosity of the injected fluid [Ns/m^2], n is the porosity of the porous medium, and α and β are the compressibilities of the porous medium and the injected fluid, [m^2/N], respectively. Rearranging, canceling terms, and solving for the pressure required to store $CO_{2(l)}$ in deep sea sediment ($P_{CO_{2,sed}}$), as a function of the mass flow rate of the $CO_{2(l)}$ ($\dot{m}_{CO_{2(l)}}$ [kg/s]), yields:

$$P_{CO_{2,sed}} = \frac{1}{4\pi} \cdot \dot{m}_{CO_2} \cdot \left(\frac{\mu}{\rho}\right)_{CO_{2(l)}} \cdot \left(\frac{1}{b\kappa}\right)_{sed} \cdot ln\left(\frac{2.25t}{r^2} \cdot \frac{\kappa_{sed}}{\mu_{CO_{2(l)}}(\alpha_{sed} + n_{sed}\beta_{CO_{2(l)}})}\right) \tag{9}$$

where r is the radius of the well [m]. Figure 2 charts (9) for typical values and parameters and conveys how the mass flow rate specific pressure ($P/\dot{m}_{CO_{2(l)}}$) increases over time.

B Elaboration of Transportation and Deep Sea Sediment Storage Cost Estimates

B.1 Pipeline Transportation Cost Estimates

The CO_2 source database includes reported and estimated emissions as well as the operating hours per year for each of over 14,650 facilities worldwide (IEA (2002*a*)). The emissions are provided in Gg/yr or, equivalently, ktonnes/year. Dividing the maximum of these emissions (either reported or estimated) by the number of operating hours for the year, and multiplying by 10^3 provides the mass flow rate $\dot{m}_{CO_2}$ for the facility in tonnes/hr.

The capital investment for an onshore pipeline is taken from (IEA (2005)), where 10 years of natural gas pipeline construction data for the US was regressed to yield \$41,681/in$_d$-mi$_L$ and combined with a rule of thumb for pipeline sizing (0.65MMSCFD/in$_a^2$) to yield an equation for the capital cost of the terrestrial pipeline that carries $\dot{m}_{CO_2}$ [tonnes/hr]: $\$39,409 \cdot (\dot{m}_{CO_2})^{0.5}$ per mile.[3] Expressing length in kilometers yields the capital cost of the onshore pipeline used in this paper:

[3]This calculation implicitly uses a density of CO_2 of 25.92 tonnes/MMSCF, or 0.915 kg/m^3.

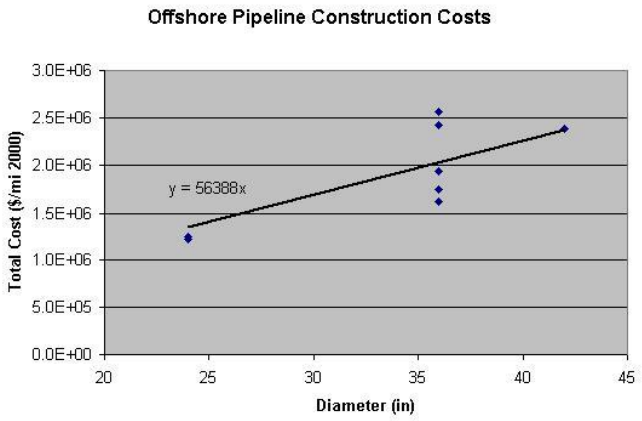

Figure 3: Offshore Pipeline Capital Investments (O&GJ (2000))

$$Cost_{PL,onshore}[\$/km] = 24,631 \cdot (\dot{m}_{CO_2})^{0.5} \tag{10}$$

This formulation and rule of thumb implicitly prescribes the allowable pipeline diameter, d_{PL} [m] for a given $\dot{m}_{CO_2}$ as:

$$d_{PL}[m] \geq \left(\frac{\dot{m}_{CO_2}}{272\pi}\right)^{0.5} \tag{11}$$

The capital investment for an offshore pipeline is based on data obtained from O&GJ (2000) for investments made in 1999 and 2000. The regression for the data shown in Figure 3 corresponds to the following capital cost for an offshore pipeline:

$$Cost_{PL,offshore}[\$/km] = 33,322 \cdot (\dot{m}_{CO_2})^{0.5} \tag{12}$$

Any fluid flowing throw a pipe will lose pressure. This pressure drop, ΔP [Pa] for the $CO_{2(l)}$ flowing through the pipeline is:

$$\Delta P = \frac{(\dot{m}_{CO_{2(l)}})^2}{\rho_{CO_{2(l)}}} \cdot \frac{f_{PL} L_{\Delta P}}{(d_{PL})^5} \cdot \frac{8}{\pi^2} \tag{13}$$

where f_{PL} is friction factor for the pipe, ρ is the fluid density [kg/m^3] , $\dot{m}$ is the mass flow rate [kg/s], and $L_{\Delta P}$ is the length of the pipeline over which the pressure drop develops [m].

The expenditure in (10) for pipeline with a diameter defined by (11) will yield the following length before the allowable pressure drop occurs and a booster station is necessary to re-pressurize and pump the flowing $CO_{2(l)}$:

$$L_{\Delta P}[km] = \frac{12.5\Delta P \cdot \rho_{CO_{2(l)}} \cdot (d_{PL})^5 \cdot (3.6\pi)^2}{(\dot{m}_{CO_{2(l)}})^2 \cdot f_{PL}} \tag{14}$$

where the units are: $L_{\Delta P}$ [km]; ΔP [bar]; $\dot{m}_{CO_{2(l)}}$ [tonnes/hr]; and the rest are as defined above.

The capital cost of a booster station, in \$M is taken from IEA (2002*b*) to be:

$$Cost_{BS}[\$M] = \$7.82W + 0.46 \tag{15}$$

where W is the energy [MW] needed to re-pressurize the $CO_{2(l)}$:

$$W[MW] = \frac{\dot{m}_{CO_{2(l)}}}{36\rho_{CO_{2(l)}}} \cdot \frac{\Delta P}{\eta_{pump}} \tag{16}$$

with η_{pump} as the efficiency of the pump, and assuming that $\dot{m}_{CO_{2(l)}}$ is in [tonnes/hr] and ΔP is in [bar].

Multiplying (16) by the number of hours and the cost of electricity [$/MWh] yields the operating cost of the booster station.

B.2 Ocean Transportation and Injection Cost Estimates

A few options for ocean disposal of CO_2 have been proposed, including dissolving in sea water by towing a pipeline from a ship and injecting it into sea water at depths greater than 3,000 m where it will form a 'lake' on top of the ocean floor. Sediment injection of CO_2 is similar to the latter option, except $CO_{2(l)}$ is injected *under* the ocean floor. $CO_{2(l)}$ can be transported to an ocean location by a pipeline laid on the seafloor or by a tanker from a port facility to an offshore floating injection facility, from which a vertical pipeline injects the $CO_{2(l)}$ into the sediment. This latter option is more likely for the locations and depths where $CO_{2(l)}$ will be injected into deep sea sediment, and relies on a combination of deep ocean injection[4] and deepwater drilling. Ocean sediment inject of CO_2 requires that CO_2 be stored at a port facility, loaded onto a tanker, transported to an offshore injection platform, and injected into a well that has been drilled into the sediment. The tanker would return, empty, to the port facility to be refilled with $CO_{2(l)}$. This appendix summarizes and reviews data and cost estimates for deep sea sediment injection of CO_2 which has been extracted from a number of sources - combining previous studies of ocean injection (forming a lake) with deepwater oil and gas industry reports, analyses, and data.

B.2.1 (Ultra)Deepwater Drilling Costs

Offshore oil and gas drilling at depths greater than -500m is generally considered 'deepwater,' whereas depths greater than -1500m are generally referred to as 'ultra-deepwater.' The frontier of offshore drilling is currently around -3,000 m water depth. Exploration wells have been drilled at depths greater than -3,000 m, and the progression of the deepest developed well has increased almost linearly since the 1980's. Activities in the Gulf of Mexico currently lead the way in increasing development depths, however there is still a lot of opportunity at 'conventional' deepwater depths which will impede the growth of activity below -3,000 m (Rowley (2004)). As of 2004, ultra-deepwater drilling was expected to account for roughly 25% of all development drilling by 2008. In the period 2004-2008, 1,348 development wells were expected to be drilled at a cost of approximately $10.2M per well, and 750 exploration and appraisal wells were expected to be drilled for an average of $27.3M per well (Rowley (2004)).

The Joint Association Survey of Drilling Costs (JAS), which is sponsored by the American Petroleum Institute, Independent Petroleum Association of America, and the Mid-Continent Oil & Gas Association, is a thorough and definitive report of drilling costs.[5] This annual survey relies on reporting from companies engaged in drilling activities and reports the estimated costs of drilling onshore and offshore wells at a variety of depths below ground and in offshore waters. Until now, however, offshore water depths have not been categorized beyond -500+ ft of water, though the next report on 2005 drilling costs (due out in November 2006) will have further classifications for water depth (including categories beyond the appropriate -10,000 ft of water).[6] It must be noted that the depths reported in the JAS combine water depth with the hole

[4]For ocean depths greater than 3,000 m, Sarv (1999) has suggested that it will be cheaper to use tankers, offshore floating platforms, and vertical pipelines for distances greater than 400 km (250 miles) instead of seafloor pipelines. Sarv (1999) also quotes two other studies that suggest this cutoff is closer to 300 km. The recent IPCC Special Report on Carbon Capture and Storage suggests that a ship transport is cheaper for distances greater than approximately 1,000 km, however this estimate is based on transporting 6Mt/yr and admittedly takes no account of ocean depth. The Sarv (1999) analysis uses, as a reference case, a 500 km one-way transportation of 181.4 $MtCO_{2(l)}$.

[5]Another definitive report appears to be the World Deepwater Market Forecast, published by Douglas-Westwood. The current version covers the period 2006-2010. This industry report is not held by any library in the United States.

[6]Obermiller, Jeff. American Petroleum Institute Contact for Joint Association Survey on Drilling Costs, Personal Communication May 3&4, 2006. obermiller@api.org, 202-682-8508.

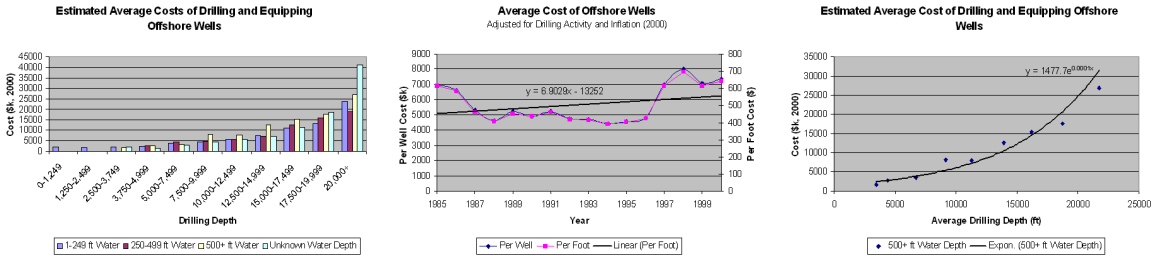

Figure 4: Estimated Average Costs of Offshore Drilling (API (2000))

depth, so that a 1,000 ft well drilled in -500 ft water is reported as a 1,500 ft well in the JAS. Since a copy of this survey costs $10,000,[7] the following information was extracted from to 2000 copy (API (2000)), which is available in the reference section of Baker Library at Harvard Business School.

Figure 4 shows the estimated costs for all offshore wells drilled in 2000. Wells drilled -3,000 m (-10,000 ft) can probably still classified as 'exploratory', given the dearth of experience at that water depth. The JAS tables indicate that offshore exploratory wells cost roughly 10-25% more than offshore production wells on average. Table 1 lists the number of exploratory wells drilled in 2000.

Drill Depth(ft)	**Exploratory Wells**	**Total Wells**	**Percentage**
0-1,249	0	2	0%
1,250-2,449	0	4	0%
2,500-3,749	2	8	25%
3,750-4,999	8	25	32%
5,000-7,499	9	53	17%
7,500-9,999	29	143	20%
10,000-12,499	48	158	30%
12,500-14,999	29	119	24%
15,000-17,499	20	63	32%
17,500-19,999	11	29	38%
20,000+	9	19	47%
Total	165	623	26%

Table 1: Offshore Wells Drilled in 2000 (Water Depth Not Available)

Figure 4(a) indicates that the average cost to drill an offshore well in 2000 was approximately $550/ft, which predicts roughly $5.5M to drill an offshore well 10,000 ft. deep, however 4(b) shows that, as expected, this expected cost is low for wells drilled in -500+ ft water. Since it is unclear how much, on average, the cost of an incremental foot of drilling depth compares to the cost of an incremental foot of water depth, and in depth analyses of the number exploratory wells versus production wells combined with the data behind Figure 4 failed to reveal any reliable pattern of trends, it is estimated that the cost to drill a shallow well in -3,000 m water is about $15M-$25M (2000).[8]

B.2.2 Tankers

Semi-refrigerated tankers that are currently used to transport liquified natural gas (LNG) can be modified to transport CO_2. These tankers travel approximately 17-20 knots (31-37 km/hr) and would likely operate

[7] The World Deepwater Market Forecast is much cheaper at a mere £2,200.

[8] Note that the information in Section B.2.5 suggests that it would cost roughly $18M to drill such a well ($200,000/day ×90 days).

just above the triple point of CO_2, around 7 bars and -50^{o}C (e.g, Sarv (1999), IPCC (2005)) where CO_2 is a liquid with a density approximately equal to 1150 kg/m^3. Most of the existing vessels have capacities of 22,000 m^3, making them capable of transporting approximately 25.3 kt of $CO_{2(l)}$, or one hour's worth of 20 GWe coal-fired power plant emissions (e.g, Sarv (1999), IPCC (2005)). Larger capacity tankers that hold 135,000 m^3 also exist, as well as a few 200,000 m^3 tankers, and could transport 155.3 and 230.0 kt, respectively, of $CO_{2(l)}$. For 500 km route to-and-from (1,000 km round trip)[9] an injection platform, thirty eight 22,000 m^3 tankers or seven 135,000 m^3 tankers will be necessary to handle the 181.4 Mt$CO_{2(l)}$/yr from the equivalent of 20 GWe of coal fired power plants (Sarv (1999)). Table 2 summarizes some of the published estimates of the cost of CO_2 transportation by refrigerated tankers.[10]

Scenario	Yearly Amount	Tanker Size	Tanker Speed	Trip Length	No. Tankers	Annual Cost	Cost
A.	5.5 Mt/yr	20 kt	35 km/hr	7600 km	17	$188M	$34/t$_{CO_2}$
B.	5.5 Mt/yr	20 kt	35 km/hr	7600 km	17	$232M	$42/t$_{CO_2}$
C.	5.5 Mt/yr	20 kt	35 km/hr	500 km	-	-	$20/t$_{CO_2}$
D.	5.5 Mt/yr	20 kt	35 km/hr	1500 km	-	-	$22/t$_{CO_2}$
E.	5.5 Mt/yr	20 kt	35 km/hr	4500 km	-	-	$28/t$_{CO_2}$
F.	-	30 kt	-	7600 km	-	-	$35/t$_{CO_2}$
G.	-	50 kt	-	7600 km	-	-	$30/t$_{CO_2}$
H.	181 Mt/yr	25.3 kt	33 km/hr	1000 km	38	-	
I.	181 Mt/yr	155.3 kt	33 km/hr	1000 km	7	-	
J.	8 Mt/yr	25.3 kt	33 km/hr	-	2(3)	-	
K.	8 Mt/yr	25.3 kt	33 km/hr	1000 km	-	-	$40-60/t$_{CO_2}$

Table 2: Previous Offshore CO_2 Ship Transportation Estimates

CO_2 tankers can be built by the same shipyards that currently build the LNG tankers. One tanker can be built in one to two years, depending on the size of the tanker. One estimate suggests that 20-30 kt$CO_{2(l)}$ tankers can be built for US$50-70M, whereas another study estimates US$34M for 10 kt$CO_{2(l)}$, US$60M for 30 kt$CO_{2(l)}$, and US$85M for 50 kt$CO_{2(l)}$ (Respectively, a 2004 communication with Statoil and IEA (2004), both cited by IPCC (2005)). Additionally, Heddle, Herzog and Klett (2003) cites a report that suggests a single 22,000 m^3 tanker would cost approximately $55M, and Ormerud et al. (2002) suggests the cost would be closer to $50M. Expected charter rates, which include capital charges, personnel, and maintenance, for a 20 kt$CO_{2(l)}$ tanker are approximately US$25,000 per day (IPCC (2005)).

B.2.3 Offshore Transportation Cost Determination Process

The total duration of a round trip for one tanker is determined by taking the total round trip distance from the port to the injection site divided by the velocity of the tanker (V_{tanker}) plus the expected times to fill and discharge a tanker at the port and injection platform (t_{fill} and $t_{discharge}$, respectively): $t_{roundtrip,tanker}[hr] = \frac{2d_{port-site}}{V_{tanker}} + t_{fill} + t_{discharge}$.

[9] Though the Exclusive Economic Zone extends roughly 200 miles from a countries' coast, tankers will not necessarily travel direct routes from the port to the storage site, and storage sites will not necessarily be located at the shortest maritime distance from a port (i.e. the port is unlikely to be located at the closest piece of land).

[10] In Table 2, scenarios A-G are from IPCC (2005), where A-E are cited from Statoil (2004) and F-G are cited from IEA (2004). A, C-E do not include liquifaction and B includes compression. According to IPCC (2005), IEA (2004) indicates a stronger sensitivity to distance than does Statoil (2004), and the IEA (2004) transportation system is 'comparable' to the Statoil (2004) system. Scenarios H and I are from Sarv (1999) and provide a $/t estimate, however the values seem to be extraneously low (e.g. $1.3/t) and cannot be reconciled. Scenario J is from Heddle, Herzog and Klett (2003) and Scenario I is from Ormerud et al. (2002). A dash '-' indicates that it is unclear what value the scenario references, but is likely to be consistent with the scenario listed above it.

One 'fleet' is defined as the number of tankers that will provide 'continuous' port coverage (i.e., as one leaves the port, another enters to be filled). Assuming that each fleet operates out of the same slip at the port or the injection platform, the fleet size will be constrained by the fill time or discharge time (whichever is greater) because two tankers cannot be filled (or discharged) simultaneously from the same slip. As a result, the number of tankers in a fleet is thus: $FleetSize[tankers] = Int\left(\frac{t_{roundtrip,tanker}}{Max(t_{fill},t_{discharge})}\right) + 1$.

B.2.4 Port Facilities

Heddle, Herzog and Klett (2003) suggest that a port facility to handle three 22,000 m^3 (25.3 kt $CO_{2(l)}$) tankers would cost approximately US$50M.

B.2.5 Offshore Rigs

Construction Costs: Heddle, Herzog and Klett (2003) cites a report wherein an offshore platform is estimated to cost approximately $200M. This platform, however, is suitable for injecting CO_2 into ocean water (the 'lake' option) and would not be equipped to drill into the ocean floor. Recent construction costs and contracts suggest that a suitable offshore injection facility could be built for approximately $500M-$600M:

- Two Japanese shipyard construction firms built the Chikyu for a total construction cost of $540 million (US) for the International Ocean Drilling Program. The Chikyu is currently capable of drilling almost 7,000 m into the ocean floor at depths up to 2,500 m (with plans to extend the capability to 4,000 m). Chikyu incorporates both the riser drilling system and dynamic positioning system (DPS). On-board research areas are located on four levels. The vessel is equipped with state-of-the-art facilities for physical, chemical, and biological analysis. Chikyu also can determine reach of the collected core, pore water, and down holes.[11]

- In 2005, Aker Drilling received a contract to build two dynamically positionable semisubmersible ultra-deepwater rigs capable of drilling at depths up to -3,000 m. The contract is for $1.2B with delivery in February and October 2008. These rigs will have dual drilling capabilities and are designed for harsh conditions. Worldwide, there are currently only 37 other ultra-deepwater rigs available, 14 of which have dual drilling capability.[12]

- In March 2006, Global SantaFe received a contract to build GSF Development Driller III (both GSF DD I & II can drill in -7500 ft deep water) for $590 million (IOD (2006)). It will be an ultra-deepwater semisubmersible capable of drilling in 10,000 m in -3,048 m deep water (Cresswell (2006)).

- A Korean firm has received an order for $550M to build a dynamically positionable ultra-deepwater drillship that will be able to drill in -3,048 deep water to depths of 1,000 m (Cresswell (2006)).

Day Rates: It can take up to 90 days to drill a complex deepwater well, which newer technologies are expected to be able to decrease drilling time to 60 days.[13] As of May 2, 2006, 50 of 54 deepwater semisubmersible rigs capable of 4,000 ft (plus water depth) drilling had an average dayrate of $194,000, and 22 of 26 drillships with the same depth ratings had an average dayrate of $187,000.[14] Dayrates for operating drillships and semisubmersible platforms have recently grown substantially past the $200,000 per day figure, with contracts for high end rigs that *begin* in 2007, 2008, and 2009 having dayrates of $300,000, $400,000 and greater than $500,000 per day.[15] In many cases, new and/or renewed contracts are $50-$100,000 per day

[11] http://www.jamstec.go.jp/chikyu/eng/index.html

[12] Aker Drilling ASA Company presentation, http://www.akerdrill.com/upload/aker_drilling_presentation_-3__final.pdf

[13] http://dnv.com/publications/dnv_forum/by_subject/oil_gas/Costeffectivedeepwaterdrilling.asp

[14] http://www.rigzone.com

[15] For example, Chevron has entered into a contract for a drillship from Transocean for 5 years, beginning in 2009, when drillship construction will be completed, for $400,000-$500,000 per day. BP will pay $520,000 per day from 2007 through 2010 for Transocean's Discoverer Enterprise drillship (PIW. (2006)). Once the new Global SantaFe Development Driller III is complete, it will be operated at $390,000 per day for seven years, and Transocean will be receiving $476,000 per day beginning in 2008 as an extension of its current contract with Reliance Industries (IOD (2006)).

more than the previous contract. These dramatic increases are likely the result of high oil prices begetting a desire for more oil production combined with the limited stock of (ultra)deepwater capable rigs.

- Short-term (1-9 month) rig dayrates for high-spec (includes 'deepwater') in 2004 were between $US 190,000 and $US 200,000/day for drillships and between $US 80,000-$US 140,000 for semi-submersibles. Long-term dayrates for semisubmersibles were between $US 90,000 and $170,000. Long-term drillship dayrates were unavailable. Source:NSL (2004).
- Dual drilling rigs can conduct two different operations simultaneously. Smedvig's 'West Navion' rig is a dual drilling rig that Amerada Hess contracted for $220,000 per day for two wells during 2002. Esso Norge paid $210,000 per day to drill into -4,430 ft deep water (Strachan (2002)).
- Of the 95 deepwater rigs operating in 2002, 29 were capable of drilling in depths greater than -7,500 ft (16 drillships, 13 semi-submersibles). Dayrates for deepwater semi-submersibles were $130,000-$195,000, and $150,000-$220,000 for dynamically positioned drillships (Strachan (2002)).

B.2.6 Injection Pipelines

A steady supply of CO_2 is necessary for offshore vertical pipelines in order to maintain a roughly constant ratio between the pressure of the flowing fluid and the external hydrostatic pressure. Due to the combination of hydrostatic pressure and corrosion possibilities, offshore pipelines must be more robust than their terrestrial counterparts and are thus more costly, however the increase in total capital expenditure is partially mitigated by much lower costs to secure rights of way.[16] According to Sarv (1999), one 64-inch (1.63 m) diameter pipeline or, equivalently, six 30 inch (0.76 m) diameter pipelines are necessary to inject 181.4 $MtCO_{2(l)}$ (200×10^6 tons $CO_{2(l)}$) per year, which is roughly equivalent to the production from 20 GWe worth of coal-burning power plants. Conceivably, once the sediment injection hole has been drilled, injection pipelines could be transferred to, attached to, and suspended from offshore platforms. Sarv (1999) state that the six 30-inch diameter pipes could be J-laid to 3,000 m long and subsequently attached to the floating platform whereas one 64-inch diameter pipe could conceptually be prefabricated onshore and towed to the offshore platform by a process that uses (lighter-than-seawater) water-filled buoys to suspend the pipe while in tow. Since the majority of the offshore pipelines constructed in 1999 and 2000 had diameters near 1 m (36" and 42" diameters), this paper uses a nominal 1 m diameter pipeline for sediment injection.

The capital cost for the offshore pipeline is based on the regression in Figure 3: $Cost_{PL,offshore}[\$/km] = 33,322 \cdot (\dot{m}_{CO_2})^{0.5}$. The pressure drop in the injection pipeline is negligible.[17]

C ArcGIS Processing

C.1 Projections

All files and layers not already in the GCS_WGS_1984 projection were projected to it for consistency. While projecting, the projection was 'imported' from the sediment thickness layer. Area calculations were performed after the requisite layers were projected to USA Contiguous Albers Equal Area Conic. Distance Calculations were performed after the requisite layers were projected to Equidistant Conic.

C.2 US Exclusive Economic Zone (USEEZ)

The three separate vector shapefiles (eastcoast_line_Project, gulf_line_WGS1984, westcoast_line_WGS1984) downloaded from Office of Coast Survey (2000) were appended to each other to create one vector shapefile, USEEZ_WGS1984.

[16] Offshore pipelines are roughly 35% more costly than onshore equivalents.

[17] The pressure drop for $\dot{m}_{CO_{2(l)}}$=855 tonnes/hr with an average density $\rho_{CO_{2(l)}}$=1100 kg/m^3 flowing 3,500 m through a 1 diameter injection pipeline, will be on the order of 0.02 bar.

1. The terminal ends of the USEEZ did not connect to the mainland.
   (a) Extracted a polygon of the United States Boundary from the Political Boundaries contained in the Global GIS CD (ESRICNTRY00).
      i. ArcToolbox, Analysis Tools, Extract, Select, FID=5810.
      ii. Saved as polygon layer, 'USBOUND_1984.'
   (b) Connected ends of US EEZ to borders with Mexico and Canada.
      i. Editor, Start Editing, Sketch Tool, Snap to End (of EEZ), Snap to Vertex (of country border).
      ii. Saved vector shapefile as 'USEEZ_WGS1984.'
2. Created a shapefile with US political boundary combined with the USEEZ: Arc Toolbox, Data Management Tools, Features, Features to Polygon.
3. Deleted the US political boundary out of the middle of the combined polygon: Arc Toolbox, Data Management Tools, Features, Delete Features.
4. Saved resulting polygon layer as 'USEEZ_Total_WGS1984.'

C.3 India Exclusive Economic Zone

The Exclusive Economic Zone for India was created by a 200 mile buffer around the Indian coast that was modified by intersection of 200 mile buffers around the coasts of neighboring countries (Pakistan, Bangladesh, and Sri Lanka).

1. Downloaded 'ESRICNTRY00' from the Harvard Geospatial Library in order to get country borders for the whole world.
2. For each of India, Pakistan, Bangladesh, and Sri Lanka, created a shapefile with a 200 mile buffer around the country. Arc Toolbox, Analysis Tools, Proximity, Buffer: Selected proper country, 200 miles, output as file '*country*Buffer.'
3. Each the country buffers were combined into one buffer file using 'union' to preserve the overlapping polygons. Arc Toolbox, Analysis Tools, Overlay, Union: Selected each *country*Buffer. Saved the resulting shapefile as 'AllBuffers.'
4. Selected polygons for Pakistan, India, Bangladesh, and Sri Lanka from ESRICNTRY00 (Select Features Tool) and 'union'ed the countries with the 'AllBuffers.'
5. Created polygons that connected the location where the outer extremity of the 200 mile buffers for two countries intersected where the border between those two countries meets the coast. Editor, Start Editing, Sketch Tool, Snap to Vertex(s) of intersecting lines for buffers and countries/coast. A similar procedure was used to essentially narrow the buffer between the Indian mainland and the island of Sri Lanka.
6. A sequence of 'union's and 'Multipart to Singlepart's (Arc Toolbox, Data Management Tools, Features) ultimately created a shapefile containing separate polygons for each portion of the buffer/country combination. Ultimately saved as 'IndiaEEZAll.'
7. Selected the polygons to be deleted (Select Features Tool) and deleted the polygons for the countries and unwanted portions of the buffers. Arc Toolbox, Data Management Tools, Features, Delete Features, 'IndiaEEZAll.' Saved shapefile as 'IndiaEEZ.'
8. Created one continual polygon for the Indian EEZ by dissolving the individual polygons together. Arc Toolbox, Data Management Tools, Generalization, Dissolve. Saved shapefile as 'IndiaEEZ.'

C.4 Density (σ) for CO_2 Storage in Worldwide Deep Sea Sediment

A raster dataset was created for the density of CO_2 at the ocean depth and sediment thickness associated with the storage of CO_2. The values in this raster must be multiplied by the available pore space in the sediment for storage and then integrated over the requisite area to yield the total quantity of CO_2 that can be stored.

1. Created a layer for the spatial overlap where the ocean depth is at least -3000 m deep and where the sediment thickness is at least 300 m. Spatial Analyst, Raster Calculator: $([WrldSedThick] >= 300)\&([WrldOcDpth] <= -3000)$. Saved as 'WrldDpthThkOK.'

2. Created raster data set for the appropriate sediment thickness for CO_2 storage over the long term.[18]

   (a) Created a layer with values of 1 if the ocean is shallower than -4000 m, and 0 if the ocean is deeper than or equal to -4000 m. Raster Calculator: $[WrldOcDpth] > -4000$. Saved as 'WDTOKDpLT4k.'

   (b) Created a layer with values for the thickness of the NBZ. Raster Calculator: $54-([WrldOcDpth]+3000)*73/270)$. Saved as 'WrldNBZThick.'

   (c) Created a layer with values for the thickness of the HFZ. Raster Calculator: $300-([WrldOcDpth]+3000)*7/250)$. Saved as 'WrldNFZThick.'

   (d) Created a layer for the appropriate sediment thickness at ocean depths deeper than -4000 m. Raster Calculator: $min([WrldSedThick],[WrldNBZThick])$. Saved as 'WrldSedGT4k.'

   (e) Created a layer for the appropriate sediment thickness at ocean depths shallower than -4000 m. Raster Calculator: $min([WrldSedThick],[WrldHFZThick])$. Saved as 'WrldSedLT4k.'

   (f) Combined 'gt4kapsd' and 'lt4kapsd': Raster Calculation: $[WrldDpTkOK]*([WDTOKDpLT4k]*[WrldSedLT4k]+(1-[WDTOKDpLT4k])*[WrldSedLT4k])$.

   (g) Exported Data in GRID format to file 'WrldSedTk4Dens.'

3. Created raster data set for the density σ as defined in Equation (4).

   (a) Raster Calculator: $[WrldSedTk4Dens]*(1011+([WrldOcDpth]+2000)/30)-[WrldSedTk4Dens]*[WrldSedTk4Dens]*11/350$.

   (b) Exported data in GRID format to file 'sigmadens.'

C.5 Area and Storable Mass in Exclusive Economic Zone

The area and storable mass in an Exclusive Economic Zone was determined for the United States as follows:

1. Created a new raster dataset for the US Exclusive Economic Zone by setting the analysis mask to 'USEEZ_Total_WGS1984.shp' (created in Section C.2) and performing a Raster Calculation where the calculation was set equal to the 'sigmadens' raster, *[sigmadens]*. The raster was saved as 'USEEZ_sigma'.

2. Created a polygon shapefile from the 'USEEZ_sigma' raster (Arc Toolbox, Conversion Tools, From Raster, Raster to Polygon). Saved as 'USEEZ_Sigma_Poly.'

3. Projected 'USEEZ_Sigma_Poly.shp' with equal area projection and saved as 'USEEZ_Sigma_Poly_Proj.shp.'

4. Added "AREA" field to the attribute table for 'USEEZ_Sigma_Poly_Proj.shp.' (Open attribute table, Options, Add Field.)

[18] Note that a number of these Raster Calculations could have been combined into one, rather than separated as presented here. I tried combining them, however the results were not correct and I could not understand where the calculations were going awry. So I did them step by step, assuring myself that the proper values were resulting from each calculation.

5. Calculated the area of each polygon using the following field calculation (selected "AREA" field from attribute table, Options, Calculate Values, Advanced):

```
DIM dblAREA as double
DIM pArea as IArea
Set pArea = [shape]
dblArea = pArea.area
```

and entering `dblArea` into the calculation box.

6. Added field "AREAOK2STO" to the attribute table and calculated the values equal to 1 if "GRIDCODE" (the density) was greater than 0.

7. Added "AREASTORE" field to attribute table and multiplied "AREA" by "AREAOK2STO" to get a field that only had the storable area in it.

8. Added field "KGCO2FULL" and calculated "AREA"*"GRIDCODE" to get the amount of $CO_{2(l)}$ that could be stored if the whole sediment thickness could be utilized.[19]

9. The attribute table was exported to a *.dbf file. Further, exported files were also produced for the West Coast, Gulf Coast, and East Coast separately by selecting the appropriate polygons and only exporting the selected records. These files were saved as `USEEZ_Sigma_Poly_Proj_'E/W/G'C_Out.dbf`.

C.6 Sediment Porosity and Permeability Maps

Future work will use DSDP, ODP, and IODP core log data to produce porosity and permeability maps of ocean sediment. The porosity map should be used in conjunction with the storable mass data derived in Section C.4. The permeability map should be used for the energy calculations in Section C.5.

C.7 USEEZ Injection Sites

Injection sites were chosen to be in the center of large areas within the column integrated storage potential map developed in Section C.5. A shapefile was created by creating a .dbf with the desired latitude and longitude data for each site. This file was added as data to the ArcGIS Map, and then 'Display XY Data.' The file was then exported as a shapefile.

C.8 US Ports

The ports listed in Table 3 were extracted from USACE (2001) based on their location (as indicated in the shapefile) and tonnage ranking from American Association of Port Authorities (2003).

C.8.1 Source to Port Distance

The distance from every point source of CO_2 to every port was determined as the as the Euclidean Cost Distance between the point source and the port location.[20]A raster for the US was created with all values set equal to 1 by using the worldwide elevation raster with an analysis mask set by a polygon for the contiguous United States and a raster calculation of the elevation value * 0 + 1. This raster was saved as 'usras_eqdcon.' To create the cost raster, some port points needed to be moved slightly so that they laid on top of the raster

[19]These values should ultimately be multiplied by the porosity map that will be developed in Section C.6, however since cursory analysis of DSDP, ODP, and IODP core data did not yield much reliable

[20]Using 'Point Distance' (Arc Toolbox, Analysis Tools, Proximity, Point Distance) creates a matrix of distances from each point in an input layer (sources) to each point in another input layer (ports) did not work correctly because it calculates a straight line distance and can thus ignores the land contours.

Port FID	Port Name (Port of)	Tonnage (tons 2003)	Ranking (US 2003)	Distance to Site 0 (West Coast)	Distance to Site 1 (Gulf Coast)	Distance to Site 2 (East Coast)
15	South Louisiana	198,825,125	1		617 km	
4	Houston (TX)	190,923,145	2		1000 km	
6	New York and New Jersey	145,889,166	3			681 km
14	Corpus Christi (TX)	77,224,732	7		1170 km	
11	Long Beach (CA)	69,195,350	8	793 km		
0	Mobile Harbor (AL)	50,214,435	14		514 km	
1	Tampa Bay (FL)	48,251,710	16		342 km	
13	Baltimore (MD)	40,183,371	19			599 km
12	Portland (ME)	29,160,899	25			1032 km
9	Portland (OR)	26,795,881	28	1000 km		
8	Charleston (SC)	25,198,899	30			670 km
3	Boston (MA)	24,832,103	31			877 km
10	Richmond (CA)	23,000,661	34	291 km		
2	Jacksonville (FL)	21,731,239	37			942 km
5	New Haven (CT)	10,385,218	51			744 km
7	Wilmington (NC)	6,810,905	65			456 km

Table 3: Selected US Ports Selected and Injection Sites

(port locations were the center of bays, for example), otherwise no distance values would be calculated. The following adjustments were made to the port locations:

1. Selected port, then Editor, Start Editing, Move, and entered the value (in meters) necessary to move it to the closest raster (North, South, East, or West).

2. Stop Editing, Save Edits.

Table 4 shows the adjustments were made to port locations:

FID	Port Name (Port of)	2003 Tonnage (tons)	2003 Tonnage Ranking (US)	Geoprocessing Adjustment
15	South Louisiana	198,825,125	1	-
4	Houston (TX)	190,923,145	2	-
6	New York and New Jersey	145,889,166	3	3 km (W)
14	Corpus Christi (TX)	77,224,732	7	4 km (S)
11	Long Beach (CA)	69,195,350	8	7 km (N)
0	Mobile Harbor (AL)	50,214,435	14	-
1	Tampa Bay (FL)	48,251,710	16	10 km (W)
13	Baltimore (MD)	40,183,371	19	2 km (W)
12	Portland (ME)	29,160,899	25	-
9	Portland (OR)	26,795,881	28	1.5 km (E)
8	Charleston (SC)	25,198,899	30	6 km (W)
3	Boston (MA)	24,832,103	31	-
10	Richmond (CA)	23,000,661	34	-
2	Jacksonville (FL)	21,731,239	37	-
5	New Haven (CT)	10,385,218	51	-
7	Wilmington (NC)	6,810,905	65	-

Table 4: Geoproccessing Adjustments for Selected US Ports

Initially, each port was selected by hand and the analysis conducted by hand. This procedure was repeated 17 times and is described below in Section C.8.2. To minimize the tedious process, a Python script that can be used for any country's data was developed. The Python code is included in Section C.8.3.

C.8.2 Source to Port Distance - Individual Ports

Each port was selected one by one and the cost-weighted a cost distance raster was created.

1. The analysis mask was set to 'usras_eqdcon' and the extent was also set to 'usras_eqdcon,' otherwise values would not be calculated for the whole extent of the raster, but rather only the extent defined by a rectangle through the most extremely located ports.

2. Cost Weighted (Spatial Analyst, Distance) rasters were created with the cost distance raster set equal to 'usras_eqdcon.' Each port was saved as '*portlabel*portdist.'

C.8.3 Source to Port Distance Automated - Python Code

```
#FILENAME: "Source to Port Distance.py"
#LOCATION: C:\Documents and Settings\Jeff Bielicki\My Documents\GIS\Data\Working Directory
#DESCRIPTION: This script determines the cost distance from each CO2 source to each port
#   and appends these distances to the CO2 source table.
#INPUTS: 1. Shapefile with port locations as points;
#   2. Raster with values equal to the cost of transporting CO2 through that raster;
#   3. Shapefile with CO2 sources as points.
#OUTPUTS: 1. A shapefile that contains appends fields with the distance to each port as well
#   as the distance to the nearest port.
#   2.  A raster with values that represent the distance to the nearest port (this is for
#   a separate study on the spatial analysis of power plant locations.
#PROCESS: A shapefile named 'Source_Port_Dist'FID'.shp' is created for each port, where FID
#   is the unique Feature ID for each port (0 - No. Ports less 1).  Fields are appended to
#   the attribute table named 'DPort'FID with values for the distance from the source
#   in the file to the port with that FID.  The output shapefile is the input to the next
#   port that is processed, and therefore the last shapefile that is created contains the
#   distances to every port.  Prior to determining 'DPort'FID, 'DPortNear' is determined and
#   represents the distance to the nearest port.  Every shapefile that is created is deleted,
#   and the last one is renamed.

print "Importing system modules."
#Import system modules
import sys, string, os, win32com.client
from win32com.client import Dispatch

print "Creating geoprocessor object."
#Create the Geoprocessor object
gp = win32com.client.Dispatch("esriGeoprocessing.GpDispatch.1")

print "Checking out licenses."
#Check out the necessary licenses
gp.CheckOutExtension("spatial")
gp.CheckOutExtension("management")

print "Loading required toolboxes."
#Load required toolboxes
gp.AddToolbox("C:/Program Files/ArcGIS/ArcToolbox/Toolboxes/Spatial Analyst Tools.tbx")
gp.AddToolbox("C:/Program Files/ArcGIS/ArcToolbox/Toolboxes/Data Management Tools.tbx")
gp.AddToolbox("C:/Program Files/ArcGIS/ArcToolbox/Toolboxes/Analysis Tools.tbx")

print "Setting up file accesses."
#Script arguments: Filenames and locations
Directory_Prefix = "C:\\Documents and Settings\\Jeff Bielicki\\My Documents\\GIS\\Data\\"
In_Port_Shape = Directory_Prefix + "US Ports\\US_Selected_Ports_EquiDist_Moved.shp" #Ports
In_Cost_Raster = Directory_Prefix + "Political Boundaries\\usras_eqdcon" #Raster w/Cost Values
In_Source_Shape = Directory_Prefix + "Worldwide CO2 Production IEA\\USA_CO2_All_EquiDist_Con.shp"  #Point Sources
Tmp_Dist_Ras = Directory_Prefix + "Working Directory\\CCS Sediment\\outgrid"  #output raster, deleted after each interation. The FID is appended to the filename for analysis.
Tmp_Dist_Shape = Directory_Prefix + "Working Directory\\CCS Sediment\\Source_Port_Dist" #Shapefile with distances attached,'FID.shp' is appended to the filename below,
Out_Dist_Ras = Directory_Prefix + "Working Directory\\CCS Sediment\\NearSrcPort"
Out_Source_Port_Dist_Shape = Directory_Prefix + "Working Directory\\CCS Sediment\\Source_Port_Dist_All.shp"

# ####This section process all of the ports simultaneously to get the distance
# ####to the nearest port.
print "Processing source to nearest port distances..."
try:  #Run the geoprocessing part
    Dist_Ras_An = Tmp_Dist_Ras + "Near" #Append "Near" to filename
    Tmp_Dist_Shape_An = Tmp_Dist_Shape + "Near.shp" #append "Near.shp" to filename
    gp.Extent = In_Cost_Raster
    gp.CostDistance_sa(In_Port_Shape, In_Cost_Raster, Dist_Ras_An, "#", "#")
    gp.ExtractValuesToPoints_sa(In_Source_Shape, Dist_Ras_An, Tmp_Dist_Shape_An, "NONE", "VALUE_ONLY")
    NewFieldName = "DPortNear" #Name a new field for the Distance to Nearest Port
    gp.AddField(Tmp_Dist_Shape_An, NewFieldName, "double")
    gp.CalculateField(Tmp_Dist_Shape_An, NewFieldName, "[RASTERVALU]")
    gp.DeleteField(Tmp_Dist_Shape_An, "RASTERVALU")
    In_Source_Shape = Tmp_Dist_Shape_An
    gp.Rename(Dist_Ras_An, Out_Dist_Ras) #Rename the distance raster
except:
    gp.AddMessage(gp.GetMessages(2))
    print gp.GetMessages(2)

print "Finished processing source to nearest port distances..."

# ####This section processes the distance to each individual port
#Get the table for the ports and get the first row
print "Processing source to individual port distances..."
rows = gp.UpdateCursor(In_Port_Shape)
row = rows.Next()

#Get the list of fields, and the first field
fields = gp.ListFields(In_Port_Shape)
field = fields.Next()

#Iterate through field names until find unique feature id FID
while field.name != "FID":
    fields.Next()

#Start a counter at first FID no. so that the excess files that are created
```

```
#(with FID appended to filename) can be deleted later.
FileCounter=row.getValue(field.name)

#Loop through each individual record in the table (each port in the shape file)
while row:
    # Create the expression to select each port one at a time
    exp = "\"" + field.name + "\" = " + str(row.getValue(field.name))
    print exp #Prints out the select statement used below
    try:  #Create a temporary in-memory layer using the expression as the definition query
        gp.makeFeatureLayer(In_Port_Shape, "tempLyr", exp)
    except:
        gp.AddMessage(gp.GetMessages(2))
        print gp.GetMessages(2)
    try:  #Run the geoprocessing part
        Dist_Ras_An = Tmp_Dist_Ras + str(row.getValue(field.name)) #Append FID to filename
        Tmp_Dist_Shape_An = Tmp_Dist_Shape + str(row.getValue(field.name)) + ".shp" #append FID.shp to filename
        gp.Extent = In_Cost_Raster
        gp.CostDistance_sa("tempLyr", In_Cost_Raster, Dist_Ras_An, "#", "#")
        gp.ExtractValuesToPoints_sa(In_Source_Shape, Dist_Ras_An, Tmp_Dist_Shape_An, "NONE", "VALUE_ONLY")
        NewFieldName = "DPort" + str(row.getValue(field.name)) #Name a new field for the PortFID
        gp.AddField(Tmp_Dist_Shape_An, NewFieldName, "double")
        gp.CalculateField(Tmp_Dist_Shape_An, NewFieldName, "[RASTERVALU]")
        gp.DeleteField(Tmp_Dist_Shape_An, "RASTERVALU")
        In_Source_Shape = Tmp_Dist_Shape_An
    except:
        gp.AddMessage(gp.GetMessages(2))
        print gp.GetMessages(2)
    gp.Delete("templyr") #Delete the in-memory layer
    gp.Delete(Dist_Ras_An) #Delete the distance raster that is created and from which values are extracted
    FileCounter=FileCounter + 1
    row = rows.Next() #Get the next row and loop
print "Finished processing source to individual port distances."

print "Deleting extraneous files..."
# #### Delete the extra files that were created
#Delete the shapefile for the nearest port
try:
    DeleteFile = Tmp_Dist_Shape + "Near.shp"
    gp.Delete(DeleteFile)
except:
    gp.AddMessage(gp.GetMessages(2))
    print gp.GetMessages(2)

#Delete shapefiles that were created for each port except the last one
for DeleteCounter in range(FileCounter-1):
    try:
        DeleteFile = Tmp_Dist_Shape + str(DeleteCounter) + ".shp"
        gp.Delete(DeleteFile)
    except:
        gp.AddMessage(gp.GetMessages(2))
        print gp.GetMessages(2)
print "Finished deleting extraneous files."

print "Renaming output file..."
try:
    RenameFile = Tmp_Dist_Shape + str(FileCounter-1) + ".shp"
    gp.Rename(RenameFile, Out_Source_Port_Dist_Shape)
except:
    gp.AddMessage(gp.GetMessages(2))
    print gp.GetMessages(2)
print "Finished renaming output file."
```

References

American Association of Port Authorities. 2003. "2003 US Port Cargo Tonnage Rankings." Industry Information - Port Industry Statistics, Online Database: www.aapa-ports.org/industryinfo/statistics.htm.

API. 2000. 2000 Joint Association Survey on Drilling Costs. Technical report American Petroleum Institute.

Cresswell, J. 2006. "Koreans Bag World's Largest Drillship." *Aberdeen Press & Journal* .

Heddle, G., H. J. Herzog and M. Klett. 2003. The Economics of CO2 Storage. Research Paper MIT LFEE 2003-003 RP Laboratory for Energy and the Environment, MIT.

House, K., D. Schrag, C. Harvey and K. Lackner. 2006. "Permanent Carbon Dioxide Storage in Deep Sea Carbonate Sediments." *Proceedings of the National Academy of Sciences* In Revision.

IEA. 2002*a*. Building the Cost Curves for CO2 Storage - Part 1: Sources of CO2. Technical Report Report Number PH4/9 International Energy Agency Greenhouse Gas R&D Programme.

IEA. 2002*b*. Transmission of CO2 and Energy. Technical Report Report Number PH4/6 International Energy Agency Greenhouse Gas R&D Programme.

IEA. 2004. Ship Transport of CO_2. Technical Report Report PH4/30 International Energy Agency Greenhouse Gas R&D Programme.

IEA. 2005. Building the Cost Curves for CO2 Storage: North America. Technical Report Report Number 2005/3 International Energy Agency Greenhouse Gas R&D Programme.

IOD. 2006. "Global SantaFe Adds to Fleet." *International Oil Daily* .

IPCC. 2005. IPCC Special Report on Carbon Capture and Storage. Technical report Working Group III of the Intergovernmental Panel on Climate Change Cambridge: .

NSL. 2004. "Rig Market Dayrates." *North Sea Letter* 6:1460.

Office of Coast Survey. 2000. "Exclusive Economic Zone." National Oceanic and Atmospheric Association; Online Database: www.ngdc.noaa.gov/mgg/sedthick/sedthick.htm. ESRI ArcGIS Interchange Coverage Format polyline shapefiles and database.

O&GJ. 2000. "Pipeline Economics." *Oil and Gas Journal* 98(36):68–86.

Ormerud, W., P. Freund, A. Smith and J. Davison. 2002. Ocean Storage of CO_2. Report IEA Greenhouse Gas R&D Programme.

PIW. 2006. "Soaring Dayrates At Last Bring New Rig Orders." *Petroleum Intelligence Weekly* .

Rowley, W. 2004. "Deepwater Drilling Analysis Suggests Significant Increase in Activity." *Offshore* 64(9):40.

Sarv, H. 1999. Large-Scale CO_2 Transportation and Deep Ocean Sequestration. Phase I Final Report DE-AC26-98FT40412 McDermott Technology, Inc.

Strachan, G. 2002. "Higher Floating Dayrates Hinge on New Round of Discoveries." *Offshore* 62(7):74.

USACE. 2001. "US Army Corps of Engineers Ports." Online Database: Harvard Geospatial Library.